

VideoPulse: Neonatal heart rate and peripheral capillary oxygen saturation (SpO_2) estimation from contact free video

Deependra Dewagiri, Kamesh Anuradha, Pabadi Liyanage, Helitha Kulatunga, Pamuditha Somarathne, Graduate Student Member, IEEE, Udaya S. K. P. Miriya Thantrige, Member, IEEE, Nishani Lucas, Anusha Withana, Member, IEEE and Joshua P. Kulasingham, Member, IEEE

Abstract—Objective: Remote photoplethysmography (rPPG) enables contact free monitoring of vital signs. It is especially valuable for neonates, since conventional methods often require sustained skin contact with adhesive probes that can irritate fragile skin and increase infection control burden. We present VideoPulse, a novel neonatal dataset combined with an end to end system that predicts neonatal heart rate (HR) and peripheral capillary oxygen saturation (SpO_2) from facial video. **Methods:** The VideoPulse dataset consists of 157 video recordings totaling 2.6 hours from 52 neonates with faces that have diverse orientations. The pipeline uses face alignment, denoising of ground-truth pulse oximeter measurements used during supervised training. Also it uses 3D CNN backbones for heart rate (HR) and SpO_2 estimation, with label distribution smoothing and weighted regression for SpO_2 . Predictions are produced in 2 second windows. **Results:** On a published neonatal dataset (NBHR), VideoPulse achieves HR Mean Absolute Error (MAE) of 2.97 bpm using 2 s windows (2.80 bpm at 6 s) and SpO_2 MAE of 1.69%. Under cross dataset evaluation, the NBHR trained HR model attains 5.34 bpm MAE on the VideoPulse dataset. For SpO_2 , fine tuning an NBHR pretrained model on VideoPulse yields MAE of 1.68%, demonstrating effective cross dataset transfer. **Conclusion:** Accurate neonatal HR and SpO_2 estimation is feasible from short (2 second) unaligned video segments, using a deep learning based rPPG pipeline with face alignment and artifact aware supervision. **Significance:** This work provides a novel neonatal dataset and algorithms that succeed even on videos with significant illumination and alignment variation, hence laying the foundation for the use of rPPG as a low cost, non invasive tool for real time monitoring in neonatal intensive care. To our knowledge, this is among the first deep learning based approaches to estimate neonatal SpO_2 from standard RGB facial video.

Index Terms—Remote photoplethysmography, neonatal monitoring, heart rate estimation, peripheral capillary oxygen saturation, pulse oximetry, facial video analysis, deep

D. Dewagiri is with the Department of Electronic and Telecommunication Engineering, University of Moratuwa, Sri Lanka and with the School of Computer Science, Faculty of Engineering, The University of Sydney, Australia.

K. Anuradha, P. Liyanage, H. Kulatunga, U. S. K. P. M. Thantrige, and J. P. Kulasingham are with the Department of Electronic and Telecommunication Engineering, University of Moratuwa, Sri Lanka.

P. Somarathne and A. Withana are with the School of Computer Science, Faculty of Engineering, The University of Sydney, Australia.

N. Lucas is with the Department of Paediatrics, Faculty of Medicine, University of Colombo, Sri Lanka.

learning, computer vision

I. INTRODUCTION

Physiological signals such as heart rate (HR), respiratory rate (RR), and peripheral capillary oxygen saturation (SpO_2) are important indicators in clinical assessment and continuous patient monitoring. Electrocardiography (ECG) and contact photoplethysmography (PPG), including pulse oximetry, are widely used to measure these signals. Remote photoplethysmography (rPPG) extends PPG to standard cameras by tracking subtle intensity variations in facial video. Those variations arise from blood volume dynamics and respiration, enabling contact free estimation of vital signs such as HR and, in some settings, SpO_2 [1]. This capability is attractive when contact sensors are impractical or increase infection control burden [2], [3]. In neonatal care, adhesive electrodes and prolonged probe contact can irritate fragile skin, motivating contact free alternatives for monitoring in the NICU and for follow up after discharge. For context, clinical monitoring standards define typical tolerance bands for these parameters. Pulse oximetry performance is commonly summarized using Arms, with a widely used benchmark of 4% over the 70 to 100% reference saturation range, while cardiac monitor standards specify allowable HR readout error of ± 5 bpm or $\pm 10\%$ of the input rate, whichever is greater [4], [5].

Early research on rPPG primarily relied on signal processing methods that analyze subtle color changes in facial regions of interest (ROI) to extract pulse related signals [6]. In practice, rPPG signals are inherently weak and are easily corrupted by motion, pose changes, illumination variation, video compression, and sensor noise. These challenges limit signal processing techniques in realistic clinical environments. To overcome these limitations, machine learning based methods have been utilized to learn spatiotemporal representations that improve robustness [7]–[12].

Recent work explores architectures that model longer temporal dependencies, including attention based models [13]. However, their computational cost and sensitivity to sequence length can be challenging for real time bedside use. More efficient sequence modeling has recently been explored using selective state space models, such as Mamba [14] and rPPG

oriented adaptations like RhythmMamba [15]. In neonatal monitoring, reliable inference from short windows and modest compute is particularly important, motivating our use of compact spatiotemporal backbones such as PhysNet [10].

Most rPPG models have been developed and validated using adult datasets, with limited research conducted on neonates. Due to the scarcity of neonatal rPPG data, existing work has focused primarily on neonatal HR estimation [16], yet HR inference from neonatal facial video remains challenging because ward recordings often contain motion and occlusion, illumination variation, and smaller usable facial regions that reduce signal quality. Evidence on neonatal SpO₂ estimation from facial video remains scarce. In addition, publicly available neonatal rPPG datasets report limited demographic and skin tone diversity [16], which restricts evaluation across broader patient populations. Since rPPG performance can vary with capture conditions and subject appearance, it is important to assess models on diverse cohorts and realistic clinical environments [17].

To address these limitations, we propose an algorithmic pipeline capable of estimating neonatal HR and SpO₂ from facial video and validate it using both public and newly collected neonatal data. We introduce **VideoPulse**, a Sri Lanka based neonatal dataset with synchronized facial video, HR, SpO₂, and pulse oximeter PPG reference signals, adding a Sri Lanka based cohort to complement existing public datasets. Compared with NBHR [16], which is the only widely used publicly available neonatal rPPG dataset, **VideoPulse** represents a different population and capture setting, with visibly different skin appearance and facial appearance typical of the Sri Lankan cohort. It motivates evaluation under population shift and domain shift. **VideoPulse** also reflects realistic ward acquisition, including in plane pose variation across three orientation bins and variable capture conditions, enabling evaluation of robustness to face orientation and alignment variability. The proposed pipeline builds upon established video based HR estimation methods and extends them to support SpO₂ prediction.

Our contributions are threefold. First, we present an end to end system that estimates neonatal HR and SpO₂ from facial video under challenging ward capture conditions, including illumination variation and unaligned faces. Second, we introduce a supervision and training strategy for SpO₂ estimation that combines pulse oximeter PPG denoising with label distribution smoothing and weighted regression to mitigate label imbalance. Third, we created the **VideoPulse** neonatal dataset with synchronized video, HR, SpO₂, and pulse oximeter PPG reference. On the NBHR dataset, our method achieves a MAE of 2.97,bpm for HR and an Root Mean Square Error(RMSE) of 2.20% for SpO₂. Under cross dataset evaluation, the NBHR trained HR model attains 5.34,bpm MAE on the **VideoPulse** dataset, and fine tuning for SpO₂ yields an RMSE of 2.18%, demonstrating effective cross dataset transfer.

II. RELATED WORK

A. Signal processing approaches in rPPG

Early rPPG pipelines relied on signal processing to recover HR from subtle color variations in facial ROI. Common

approaches include Plane Orthogonal to Skin (POS) and CHROMinance based rPPG(CHROM) style color projection methods [18]–[23], as well as decomposition based techniques such as Principle Component Analysis(PCA) and Independent Component Analysis(ICA) [6], [20], [21], [24]–[30]. These methods can perform well under stable illumination and limited motion, but performance often degrades under realistic conditions due to motion, pose changes, illumination variation, occlusion, and video compression [31].

B. Machine learning Approaches in rPPG

Machine learning based rPPG methods estimate HR by learning spatiotemporal representations from facial videos. Early models used 2D convolutional networks [7], [8] but struggled to capture temporal dynamics. This led to 3D convolutional approaches [9]–[11] that better model periodic signals in short video sequences. Attention based designs such as convolutional attention networks further improve robustness by focusing on informative spatiotemporal regions [2], [32]. Transformer based rPPG models that can capture longer range dependencies have also been explored, such as TransRPPG and EfficientPhys [33], [34], while PhysFormer models rPPG features using video transformer attention [13]. More recently, RhythmMamba leverages selective state space modeling to capture periodic patterns efficiently [15], building on the Mamba sequence modeling architecture [14].

C. Camera based SpO₂ estimation

Compared with HR estimation, camera based estimation of SpO₂ is less mature and remains challenging because it depends on wavelength specific absorption and requires stable estimation of pulsatile and baseline components under noise. One recent study estimate SpO₂ from videos using spatiotemporal map representations and an EfficientNet B3 style backbone with a regression head [1]. Other approaches first estimate rPPG representations from facial or hand regions and then use temporal models, such as a CNN BiLSTM pipeline, for SpO₂ prediction [35]. However, further evaluation of such models under realistic motion and illumination conditions, and across diverse cohorts is required.

D. Impact of illumination and skin tone

Recently, researchers evaluated the potential bias of rPPG methods with respect to skin tone using a series of hypothesis tests [17]. To support this investigation, they developed a dedicated dataset consisting of video recordings of participants from India and Sierra Leone that were captured under carefully controlled conditions with limited motion and illumination variation. Using this dataset, several state-of-the-art rPPG algorithms were assessed to determine whether geographic or demographic variations influenced performance. The analysis revealed no statistically significant differences in mean pulse rate distributions between the Indian and Sierra Leonean participants. This result indicates that, under well-controlled capture conditions, the evaluated rPPG approaches do not exhibit measurable bias toward different countries or skin tones.

However, controlled capture settings do not fully represent neonatal bedside video with motion, occlusion, and variable illumination, so evaluation across diverse cohorts and realistic clinical conditions remains important.

E. Neonatal specific datasets and studies

Most rPPG methods have been developed for adults, and fewer studies target neonatal monitoring. NBHRnet [16] is a notable neonatal HR estimation model evaluated on the NBHR dataset, using Kernelized Correlation Filters for region tracking and data augmentation for robustness. Additional neonatal datasets from different clinical environments and populations are important to assess external validity, including potential cohort shifts related to capture conditions, facial characteristics, and skin tone distribution.

Prior work on neonatal oxygenation from cameras has largely focused on feasibility in the NICU and on signal processing or calibrated regression rather than end to end deep learning. Early NICU studies demonstrated continuous noncontact vital sign monitoring in preterm infants from video, including SpO₂ related measurements alongside heart and respiratory signals. These also highlight practical limitations such as motion, occlusion, and variable illumination in real bedside settings [36], [37]. More recent efforts have explored camera based estimation of oxygenation using optical or hardware assisted setups and clinical calibration, for example a notch RGB camera clinical trial that reports continuous SpO₂ estimation in the NICU [38]. Related pediatric and neonatal camera based studies also report simultaneous estimation of oxygenation and pulse related signals, including percutaneous arterial oxygen saturation and tissue oxygen saturation, but generally rely on classical rPPG feature extraction and calibration rather than deep learning models trained to infer SpO₂ directly from RGB video [39]. Overall, compared with neonatal HR estimation, neonatal SpO₂ estimation from standard RGB facial video remains less explored, and challenges such as weak pulsatile content, frequent motion, face visibility constraints, and noisy pulse oximeter supervision motivate more robust learning based approaches [40].

F. Addressing label imbalance in SpO₂ estimation

Imbalanced target distributions are common in regression tasks where labels concentrate around a narrow range. Such imbalances are common for SpO₂ in clinical data where labels cluster near high saturation values. Deep imbalanced regression methods address this by smoothing label distributions and reweighting samples so that the model learns effectively across the full target range. Label distribution smoothing is a practical approach that accounts for nearby target values during training and can improve calibration in continuous prediction tasks [41].

Although numerous deep learning models have been proposed for the estimation of HR from adult videos, with comparatively fewer targeted at neonates, research on the prediction of SpO₂ remains limited. Only a small number of models have been developed for adults, and as per our knowledge, no deep learning models have addressed SpO₂ prediction in neonates.

III. METHODOLOGY

The proposed neonatal HR and SpO₂ prediction pipeline is shown in Fig. 1. Two previously published datasets were used [16], [42] in addition to our own novel dataset. The datasets consist of RGB facial videos paired with ground truth data, including HR and PPG waveforms obtained through contact-based measurement devices. In some cases, the datasets also include ground-truth measurements of SpO₂ levels [16], [31], [42]. Section IV provides more details about these datasets.

A. Preprocessing

A shared preprocessing pipeline was applied for both neonatal HR and SpO₂ estimation. Each input video was segmented into two second clips (60 frames at 30 fps). For each clip, we localized the face using a YOLOv5 face detector pretrained on adult face datasets. To reduce computation and stabilize the region of interest, we first attempted face detection on the first frame. If detection was unsuccessful, the pipeline advanced by 30 frames and retried, repeating this process until a valid bounding box was obtained. Once a face was detected, the same bounding box was applied to the remaining frames of the clip. If the bounding box was lost, the system again scanned forward in 30 frame steps until a valid detection was recovered and then updated the bounding box.

Neonatal recordings often contained rotated faces due to spontaneous motion and camera placement. Therefore, prior to cropping, clips were rotated in 90° increments and the same face localization procedure was repeated until the detector produced a valid face localization. The detected facial region was then cropped and resized to 128 × 128.

After alignment and cropping, temporal difference normalization was applied to emphasize subtle pulse related intensity variations while suppressing static appearance and lighting bias. Specifically, we computed differences between consecutive frames and normalized these differences by their standard deviation, producing a standardized input sequence used consistently across all datasets.

B. Heart Rate Prediction

Neonatal HR prediction was performed using the PhysNet 3D CNN trained on the NBHR neonatal dataset. Although RhythmMamba [15] showed strong performance on adult datasets in our preliminary experiments, it did not transfer reliably to neonatal videos. Hence, PhysNet [10] was selected for the final system. For training, we utilized the negative Pearson correlation loss [43] to measure the correlation between the ground-truth and predicted rPPG waveforms.

1) *Face Alignment*: To enhance the performance of the Physnet model, we included a face alignment module. Unlike adult subjects, who can maintain a stable and consistent pose during video capture, neonates frequently exhibit spontaneous movements, making it challenging to obtain properly aligned facial videos. In many instances, neonatal videos may be captured at rotated angles due to their unpredictable motion or camera positioning.

To address this, we introduced a face alignment step prior to feeding video frames into the model. For face detection, we

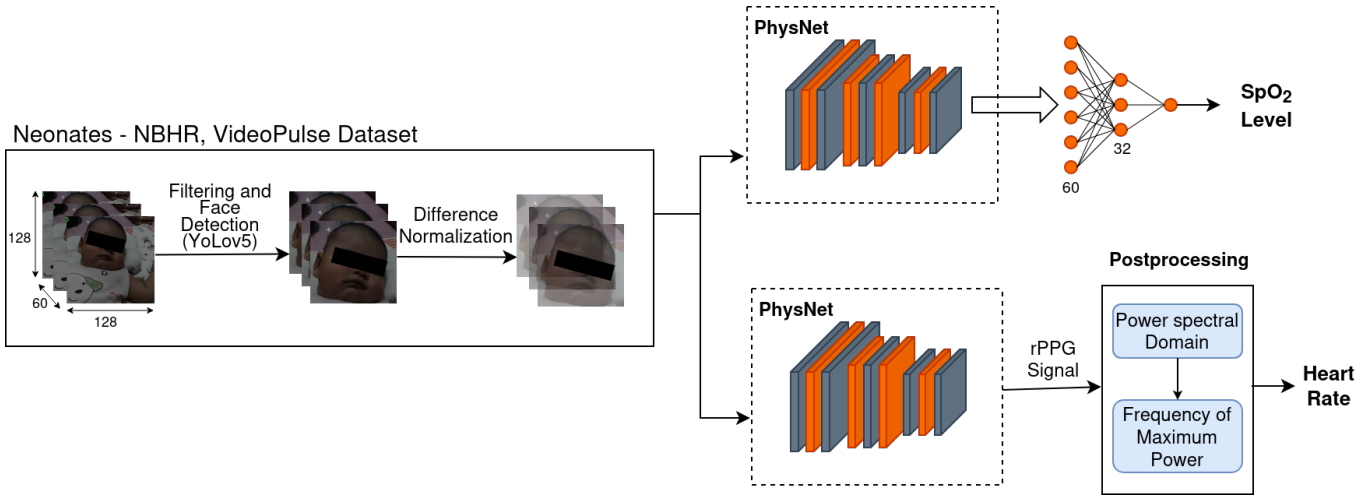


Fig. 1: System architecture. The proposed HR and SpO₂ prediction pipeline is shown for both adults (only SpO₂), and neonates (both SpO₂ and HR). The model was trained the NBHR dataset for neonates and further fine-tuned on the VideoPulse dataset.

compared RetinaFace [44], [45] with a ResNet 50 backbone [44], [46] against a YOLOv5 based face detector pretrained on adult face datasets. While RetinaFace failed to perform reliably on our neonatal videos, the YOLOv5 detector produced more stable detections on neonatal faces without additional fine tuning [44]. In our implementation, the detector attempts to localize the face in the first frame; if unsuccessful, it advances by 30 frames and retries until a bounding box is found. Once detected, the same bounding box is applied to the remaining frames of the 2 second clip, after which difference normalization is performed. A limitation of the detector is that it is most reliable for upright faces, so we leveraged detection failure as an alignment check. Since neonates in our videos were not always upright, when no face was detected, the video was rotated in 90° increments until detection succeeded. However, the method does not perform well when the face is tilted at intermediate roll angles, for example around 45°, which remains a limitation of this approach.

2) Ground truth PPG denoising: In neonatal monitoring, the acquisition of clean ground truth PPG data is particularly challenging. Unlike adults, neonates are active during data collection, often leading to significant motion-induced artifacts in the PPG signals. Although pulse oximeter probes specially designed for neonates were used in both the NBHR and our own VideoPulse datasets, there was high level of noise due to motion in the recorded ground truth signals compared to adult datasets.

To address this issue, we implemented a PPG reconstruction pipeline based on established GAN architectures for signal denoising. Low quality segments of the ground truth PPG waveform were identified using a one class Support Vector Machine (SVM) that has been widely used for PPG signal quality assessment [47], [48]. In this work, we adopted the pretrained SVM model and its inference procedure provided by prior work, and applied it to our recordings using sliding window segmentation with 30 second windows and a 2 second shift, resulting in a 28 second overlap between consecutive windows (about 93.3% overlap). Noisy segments shorter than

a predefined threshold (15 seconds) were then processed using a pretrained GAN based reconstruction model from prior work [47], [49], [50]. We used the released pretrained generator and discriminator for reconstruction, where the generator estimates cleaned windows and the window is advanced by the same 2 second shift for iterative reconstruction. This supports denoising while preserving HR related features such as peak timing and waveform shape.

Following reconstruction we applied a filtering algorithm to further refine the PPG signal, as shown in Fig.2. Heart rate variability (HRV) was analyzed within sliding windows of 2 seconds. If a window exhibited abnormal variability, defined as a fluctuation greater than 15 bpm, it was marked as noisy and excluded from the final training and evaluation set. The corresponding 2-second video clips were also discarded to ensure consistency between input videos and ground-truth signals. This step was particularly important because neonatal movement, such as hand motion, often causes artifacts in the pulse oximeter readings used as ground truth, leading to unreliable PPG segments that could degrade model performance.

To measure similarity between the predicted rPPG waveform and the ground truth PPG waveform, we use the negative Pearson correlation loss. For each input clip, let $s_{pre}, s_{gt} \in \mathbb{R}^T$ denote the predicted and ground truth waveforms over T temporal samples. The Pearson correlation is computed along the temporal dimension and the loss is averaged over clips in the minibatch:

$$L_p = 1 - \frac{\sum_{t=1}^T (s_{pre,t} - \bar{s}_{pre})(s_{gt,t} - \bar{s}_{gt})}{\sqrt{\sum_{t=1}^T (s_{pre,t} - \bar{s}_{pre})^2} \sqrt{\sum_{t=1}^T (s_{gt,t} - \bar{s}_{gt})^2} + \epsilon}, \quad (1)$$

where \bar{s}_{pre} and \bar{s}_{gt} are temporal means and ϵ is a small constant for numerical stability.

3) Post-processing: Postprocessing steps were then applied to extract the HR from the predicted rPPG signal. According to prior research, there are two primary methods [13], [43] for extracting HR from PPG or rPPG signals:

- 1) Peak detection: Identifying peaks in the rPPG signal to calculate the interval between successive heartbeats.

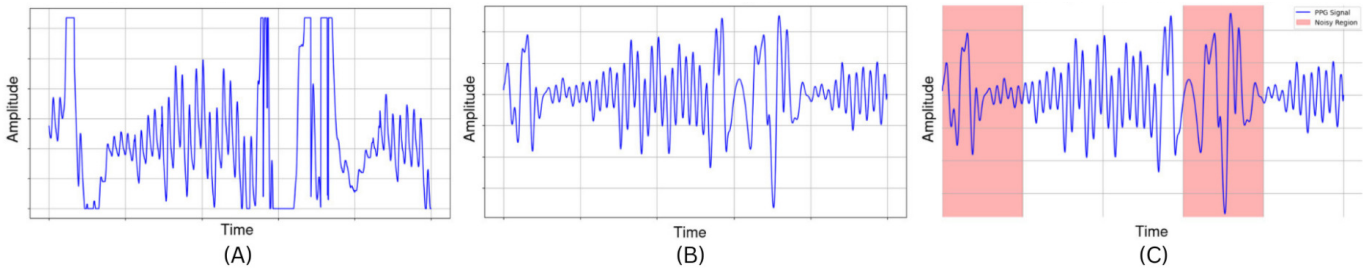


Fig. 2: Ground truth PPG denoising. **A:** Raw PPG signals from the oximeter containing motion artifacts. These are first classified by an SVM to identify noisy regions. **B:** The reconstructed signal after the noisy segments were reconstructed using a GAN. **C:** The reconstructed signal is further filtered to recover clean PPG segments for reliable rPPG analysis. The red shaded regions are removed since they are too noisy.

- 2) Frequency analysis: Analyzing the Power spectral density (PSD) of the rPPG signal to determine the dominant frequency component corresponding to the HR.

In our approach, we employed the PSD method for HR extraction. Initially, a second-order Butterworth bandpass filter with a cutoff range of 0.4 Hz to 4 Hz was applied to the rPPG signal to isolate the relevant frequency components. Subsequently, we performed a Fast Fourier Transform (FFT) on the filtered signal to compute its power spectral density. The HR was then extracted as the frequency component with the highest power.

C. Blood Oxygen Saturation Prediction

For predicting SpO₂ levels, we experimented with several approaches, including the use of spatiotemporal maps with an EfficientNet-B3 backend, RhythmNet, PhysFormer, PhysNet, RhythmMamba, and VideoMamba [10], [13], [15], [51]–[53]. These methods utilize a range of backbone architectures, including 2D CNNs, 3D CNNs, Vision Transformers, and Vision Mamba [14]. Among them, PhysNet demonstrated the best performance in SpO₂ prediction, leveraging 3D CNNs for effective spatiotemporal feature extraction.

1) *Modified PhysNet Model for SpO₂ Prediction:* We adapt PhysNet for SpO₂ regression by appending a three layer fully connected head to the final PhysNet representation. Specifically, two hidden layers of 60 and 32 neurons are used with ReLU activations, followed by a single neuron linear output layer for continuous SpO₂ prediction. The model was trained using the RMSE loss function, which is well-suited for continuous regression outputs.

2) *Neonatal SpO₂ Prediction:* We also trained the PhysNet model using the NBHR dataset after incorporating the filtering step we mentioned in Subsection III-B.2. The same preprocessing pipeline used for HR prediction was applied to the SpO₂ prediction task to ensure consistency in data preparation. The NBHR dataset [16] exhibits a right-skewed distribution (more SpO₂ values near 100%) with notable label imbalance. To mitigate the effects of label imbalance, Label Distribution Smoothing (LDS) [41] was applied using a Beta kernel with kernel size $k_s = 7$ and shape parameters $\alpha = 2$ and $\beta = 5$, resulting in a smoother and more continuous approximation of the empirical label distribution. The resulting smoothed distribution was used to compute sample-wise weights that guide the learning process.

To further enhance generalization, particularly given the temporal nature of the data, we employed a Time Reversal preprocessing technique. In this approach, each video input sequence was reversed along the temporal dimension and then fed into the model as an additional training sample. This augmentation enables the model to capture temporal patterns more robustly by learning from both the original and time-reversed sequences.

For SpO₂ regression we trained with a Weighted RMSE objective to mitigate label imbalance. In our training data, normal saturation values occur far more often than low saturation values; optimizing standard RMSE can therefore under emphasize errors in rare but clinically relevant ranges. We compute sample weights from the smoothed label distribution (LDS) estimated on the training set, assigning larger weights to rarer labels. The loss is

$$L_{\text{wRMSE}} = \sqrt{\frac{\sum_{i=1}^N w_i (s_{\text{pre},i} - s_{\text{gt},i})^2}{\sum_{i=1}^N w_i + \epsilon}}, \quad (2)$$

where N is the number of samples in a mini batch, $s_{\text{gt},i}$ and $s_{\text{pre},i}$ are the ground truth and predicted SpO₂ values for sample i , and w_i is the LDS derived weight for the corresponding label. We normalize the weights so that their mean is 1, which preserves the scale of the loss. The loss has the same unit as the target, here percent SpO₂.

For the VideoPulse dataset that we collected, we initialized the model using a pre-trained checkpoint obtained from training on the NBHR dataset. To retain the general spatiotemporal representations learned from the NBHR dataset, we froze the top two 3D convolutional layers of the model during fine-tuning. The remaining layers were then fine-tuned using the VideoPulse dataset to adapt the model to the new domain.

3) *SpO₂ Prediction on an Adult Dataset:* Our pipeline was further evaluated on a well-known adult rPPG dataset [42]. For this experiment, face detection was performed using the Haar Cascade method. The PURE dataset was divided into 70% for training, 10% for validation, and 20% for testing. The same model architecture used in the neonate experiments was employed for this evaluation.

Performance on the PURE test split achieved a MAE of 0.97 for SpO₂ prediction.

D. Model Implementation Details

All models in the proposed pipeline were implemented using the PhysNet architecture. The input to the network consisted of RGB video clips of size $128 \times 128 \times 60$, corresponding to spatially normalized facial regions over a temporal window of 60 frames.

For HR prediction, the original PhysNet architecture was used without structural modification. For SpO₂ prediction, the PhysNet backbone was retained, and additional fully connected layers were appended to the original model output. The PhysNet model produces a feature representation with 128 neurons at the output stage. To adapt this representation for SpO₂ estimation, two additional feed-forward layers with 60 and 32 neurons, respectively, were added, followed by ReLU activation functions. A final fully connected layer with a single neuron and linear activation was used to produce continuous SpO₂ predictions.

The models were trained using the NBHR dataset with a dataset split of 70% for training, 15% for validation, and 15% for testing. We did not use VideoPulse for training; instead, we used it for finetuning and evaluation to quantify generalization to unseen neonatal data.

Training was performed on a system equipped with an NVIDIA RTX 4090 GPU. The models were trained for 27 epochs using an initial learning rate of 0.01. To improve convergence and stabilize training, the OneCycleLR learning rate scheduler was employed, allowing the learning rate to vary dynamically during training.

All preprocessing steps, including face detection, alignment, difference normalization, and filtering, were applied consistently across training, validation, and testing datasets to ensure fair evaluation and reproducibility.

IV. DATASETS

A. Dataset Overview

We used NBHR and VideoPulse rPPG neonatal datasets for training and testing. Our model pipeline was also trained and tested on the PURE [54] dataset with adult rPPG. A brief descriptions of the datasets used in this study are given below.

NBHR consists of 1130 videos and reference vital signs that are recorded from 257 infants at 0–6 days old. The facial videos and corresponding synchronized physiological signals including photoplethysmography information, HR and SpO₂ level are recorded.

PURE is a benchmark rPPG dataset consisting of 10 adult subjects recorded over 6 sessions. Each session lasted approximately 1 minute, and raw video was recorded at 30 fps. The 6 sessions for each subject consisted of: (1) steady, (2) talking, (3) slow head translation, (4) fast head translation, (5) small and (6) medium head rotations. Pulse rates are at or close to the subject’s resting rate.

B. The VideoPulse dataset

To our knowledge, NBHR [16] is the only widely used publicly available neonatal rPPG dataset that includes facial video with synchronized HR and SpO₂. As a single site

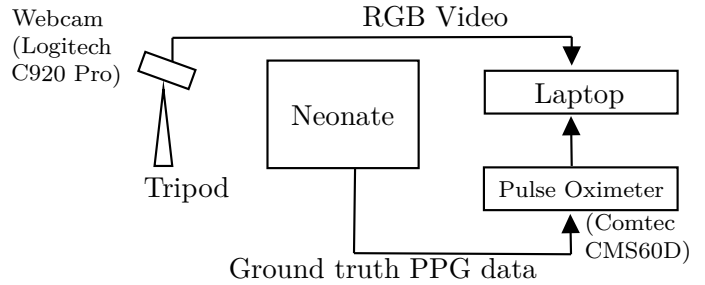


Fig. 3: Schematic of the VideoPulse data collection setup. A webcam mounted on a tripod records RGB video of the neonate in synchronization with a pulse oximeter measuring ground truth PPG data.

dataset, it provides limited demographic coverage, motivating collection of additional neonatal data from other populations and clinical environments. Due to the limited availability of diverse data, collecting our own dataset was essential. Data collection was performed after obtaining ethical clearance from the Ethics Review Committee of the University of Moratuwa, Sri Lanka, and the Ethics Review Committee of the De Soysa Maternity Hospital, Sri Lanka. Written consent was provided by the parents of all neonatal subjects. All collected data was anonymized to remove personal information.

Data were collected using an overhead, downward facing Logitech C920 HD Pro webcam (1080p, 30 fps, 78 degree diagonal field of view, autofocus) mounted on a tripod with a horizontal boom arm, together with a neonatal pulse oximeter. Both devices were connected to a single PC to acquire time synchronized facial video and pulse oximeter PPG signals (Fig. 3). Reference PPG waveforms were recorded using a Contec CMS60D pulse oximeter. Additionally, we developed a simple application in C++ to simultaneously record the raw video feed from the camera and the ground truth signals, ensuring both were aligned in the same global time frame. The videos were recorded at 30 fps, while the ground truth data was sampled at 60 Hz. **VideoPulse** consists of 157 video recordings collected from 52 neonates (postnatal age 0 to 6 days) in the postnatal ward of a partner hospital. The cohort included 25 male and 27 female neonates, with mean postnatal age 4.77 days. Tables I and II present a summary of the **VideoPulse** dataset. Due to privacy concerns regarding facial videos, the dataset cannot be made publicly available but will be provided to researchers when requested by the authors.

To reduce reliance on upright face alignment and to better reflect real ward viewing conditions, we intentionally captured sessions with in plane head orientation variation. Recordings were obtained across three predefined orientation bins, introducing rotational pose diversity that supports evaluation of robustness to face orientation and alignment variability.

V. RESULTS

Results are summarized using MAE, RMSE, MAPE, and SD (standard deviation of the error). We also report TW, the prediction time window length, in seconds to reflect latency. SD summarizes variability, and TW is reported in seconds to indicate latency. For HR, errors are expressed in beats per

TABLE I: Summary of neonatal VideoPulse dataset

Description	Value
Total number of neonates	52
Number of male neonates	25
Number of female neonates	27
Male to female ratio	25:27 (0.93:1)
Mean postnatal age at recording (days)	4.77
Total video length (h)	2.60
Total number of recording sessions	157
Average video length per session (s)	69
Number of videos of each recording scenario	2, 3
Age (days)	0 to 6

TABLE II: VideoPulse dataset statistics

Metric	Mean	Std. dev.	Min	Max
SpO ₂ (%)	94.45	2.80	87	99
Heart rate (bpm)	113.99	13.96	79	174

minute (bpm), and for SpO₂, errors are expressed in percent saturation (%). For MAE, RMSE, MAPE, and SD, smaller values indicate better performance. Best values in each column are highlighted in bold, and the symbol ↓ indicates that "lower is better".

A. Neonatal Heart Rate Estimation

The proposed approach is evaluated against several state-of-the-art methods in neonatal HR prediction from videos, including two data-driven approaches and three signal-processing-based methods, namely: CHROM, 2SR, POS, EVM-CNN, PRNet and NBHRnet. We achieved promising results in the task of neonatal HR prediction as shown in Table III when testing on the NBHR dataset. Our proposed method demonstrated the best performance compared to both data-driven deep learning models and traditional signal processing approaches. Notably, our model achieved the best accuracy while using shorter time window video clips (compared to the state-of-the-art). For the NBHR dataset we achieved a best performance of 2.80 MAE (bpm) and 2.44 MAPE % for the 6s window and the lowest values of SD (bpm) for 4s. This suggests that our approach not only improves prediction accuracy but also reduces latency in HR monitoring, which is especially valuable in neonatal care settings where timely and accurate monitoring is critical.

In addition to that, we obtained reasonable results for our own VideoPulse dataset. Here, we trained the models on the NBHR dataset and then fine-tuned and evaluated them on the VideoPulse dataset. Table IV summarizes the SpO₂ and heart rate ranges observed in the VideoPulse dataset. As shown in Fig. 4, our predictions closely track the reference on the NBHR test split, with errors centered near zero.

B. Neonatal SpO₂ Estimation

This section presents the experimental results for SpO₂ estimation on both adult and neonatal datasets. Performance metrics used include RMSE and MAE, which are standard for regression tasks in physiological signal estimation.

1) *Neonatal SpO₂ Prediction on the NBHR and VideoPulse Dataset*: In this section, we focus on the neonatal population for SpO₂ estimation, which has received limited attention in prior research. To the best of our knowledge, this work constitutes the first attempt to predict SpO₂ levels in neonates using a video-based deep learning approach. We initially evaluate our modified PhysNet model on the publicly available NBHR dataset. Subsequently, we fine-tuned the model using our own neonatal video dataset, VideoPulse. As shown in Fig. 5, the predicted SpO₂ closely follows the reference on both NBHR and VideoPulse, with most points near the $y=x$ line. Table V presents the performance of our method on both datasets.

2) *Ablation Study*: An ablation study (see Table VI) was conducted on the NBHR dataset to assess the effect of different training strategies. The architecture (PhysNet 3D-CNN), optimizer, training budget, and NBHR split were held constant and only the training strategy was varied. Using only RMSE yields an SpO₂ RMSE of **2.74**, and this is considered the baseline. Replacing it with the label-distribution-smoothed weighted RMSE (LDS-WRMSE) reduces the RMSE to **2.30** (-0.44 absolute change; -16.1% change vs. baseline). Adding time-reversal augmentation further reduced RMSE to **2.20** (additional -0.10; -19.7% vs. baseline). NBHR labels are concentrated around normal saturations, so optimizing plain RMSE tends to prioritize the majority region and can bias errors on less frequent values. LDS weighted RMSE rebalances the contribution of each label region using a smoothed estimate of label frequency, which reduces this imbalance driven bias and improves overall RMSE. Time reversal further acts as a regularizer: over short windows the rPPG waveform is approximately quasi periodic, and reversing the sequence preserves morphology while discouraging reliance on direction specific temporal artifacts such as motion trends, improving generalization.

C. Adult SpO₂ Estimation

Table VII shows the performance of different models on the PURE dataset for adult SpO₂ estimation. Methods such as ST Maps with EfficientNetB3, RhythmMamba, CNN-based, and ViM-based models were evaluated. The modified PhysNet architecture with 3D convolutional layers significantly outperformed all other state-of-the-art models, achieving an RMSE of 0.96. Although the focus of this work is neonatal prediction, this result is reported to highlight the suitability of our approach even for adult SpO₂ estimation.

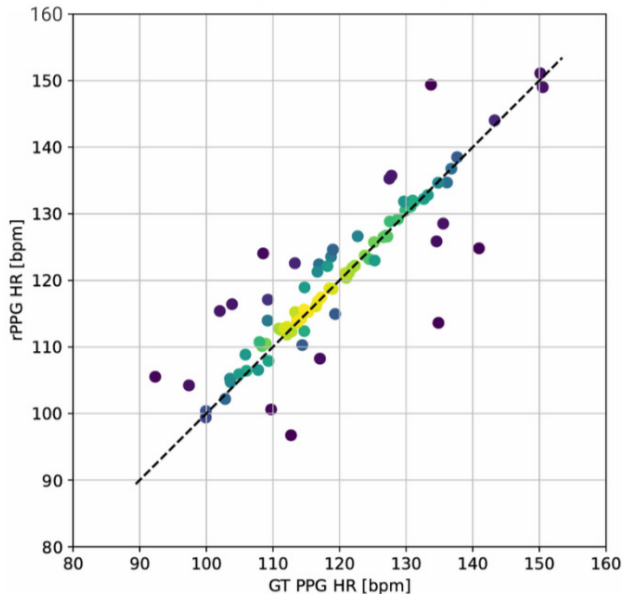
VI. DISCUSSION

This work is, to the best of our knowledge, the first to estimate neonatal SpO₂ directly from video using DeepLearning. We also contribute the following advances to the rPPG domain:

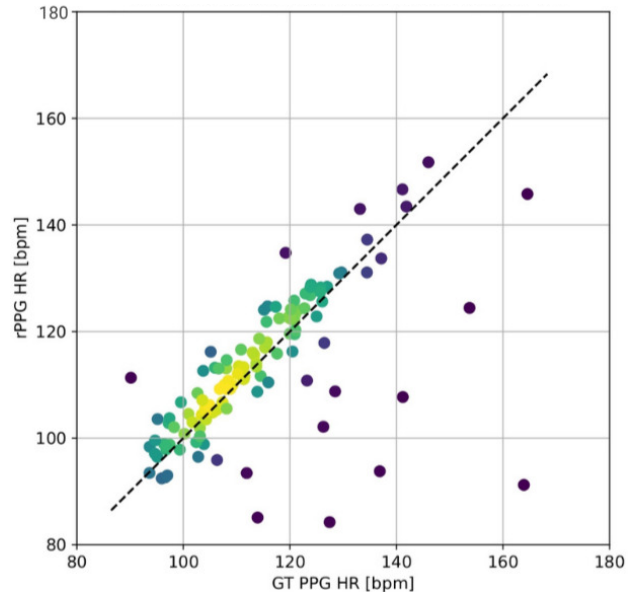
- the introduction of a GAN-based ground-truth PPG reconstruction strategy for neonates;
- the application of label-distribution smoothing to correct target imbalance in SpO₂ prediction; and
- the creation of **VideoPulse**, the second neonatal rPPG dataset.

TABLE III: Heart rate estimation comparison for NBHR dataset

Method	MAE (bpm) ↓	SD (bpm) ↓	MAPE (%) ↓	TW (s)
CHROM	6.34	8.02	5.49	12
2SR	5.48	7.69	4.93	6
POS	5.96	10.93	5.12	10
EVM CNN	4.51	5.78	3.91	8
PRNet	5.66	7.83	4.74	2
NBHRnet 2 s	3.97	5.32	3.28	2
NBHRnet 4 s	3.83	5.16	3.20	4
NBHRnet 6 s	3.76	5.15	3.13	6
Ours 2 s	2.97	5.36	2.64	2
Ours 4 s	2.89	5.12	2.45	4
Ours 6 s	2.80	5.23	2.44	6
Ours 8 s	3.23	5.19	2.83	8



(a) Comparison between reference and predicted HR of NBHR dataset.



(b) Comparison between reference and predicted HR of VideoPulse dataset.

Fig. 4: Neonatal Heart Rate estimation results. **A**: Evaluation on the test split of NBHR dataset. **B**: Evaluation on the test split of VideoPulse dataset. Predictions align closely with the identity line and errors remain centered near zero.

TABLE IV: Heart rate estimation on VideoPulse dataset

Method	MAE (bpm) ↓	SD (bpm) ↓	MAPE (%) ↓	TW (s)
Ours	5.34	7.12	4.32	2

On the NBHR dataset, our pipeline reduces heart-rate MAE to **2.97 bpm**, representing a **21 %** improvement over the previous state-of-the-art NBHRnet-6s model (3.76 bpm), while matching or slightly reducing MAPE (3.04 % vs. 3.13 %). For SpO₂, we achieve an RMSE of **2.20 %** saturation on NBHR and **2.18 %** saturation on **VideoPulse**. All predictions are generated in 2-second windows, reducing inference latency compared with the 6-second windows used in prior work and paving the way for near-real-time neonatal monitoring in the NICU.

The **VideoPulse** dataset consists of video recordings and synchronised pulse oximeter signals collected from 52

neonates. The dataset contains 157 video clips with a total duration of approximately 2.6 hours. To date it represents one of the largest neonatal rPPG datasets with ground-truth vital signs (HR, SpO₂ and PPG signals).

Future work will focus on scaling data collection across multiple hospitals and ethnic groups, improving resilience to motion and ambient lighting, and further reducing estimation error. By delivering sub-clinical-error and two-second-latency estimates of both HR and SpO₂ from a standard webcam feed, this study moves contact-free neonatal monitoring a decisive step closer to routine clinical integration.

VII. CONCLUSION

This work introduces **VideoPulse**, a neonatal rPPG dataset and the first end-to-end pipeline that jointly estimates neonatal HR and SpO₂ from video. By combining YOLO-guided face alignment, GAN-based signal reconstruction, and label-distribution smoothing with a weighted-RMSE loss, the system

TABLE V: Neonatal SpO₂ estimation results

Method	Dataset	MAE(%)↓	RMSE(%)↓
Notch RGB camera with calibration [38]	Clinical NICU preterm cohort (n=22)	3.41 to 3.17	NR
Ours	NBHR	1.69	2.20
Ours	VideoPulse	1.68	2.18

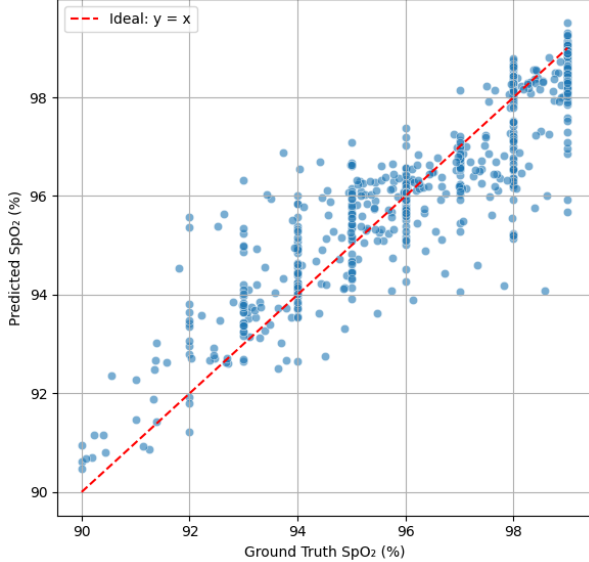


Fig. 5: Neonatal SpO₂ estimation on the NBHR dataset. The scatter plot of predicted vs. ground truth values is shown with the red dashed line indicating the ideal $y = x$ reference. The predicted values have a reasonable correspondence with the ground truth values.

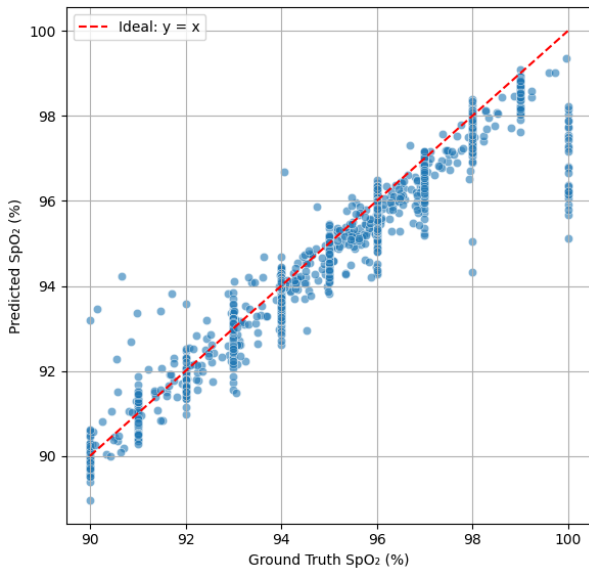


Fig. 6: Neonatal SpO₂ estimation on the VideoPulse dataset. The scatter plot of predicted vs. ground truth values is shown with the red dashed line indicating the ideal $y = x$ reference. The predicted values have a reasonable correspondence with the ground truth values, although there are some outliers at 100% ground truth saturation.

demonstrates the feasibility of reliable non-contact monitoring for neonates. Importantly, the model produces accurate predictions from very short time windows, surpassing state-

TABLE VI: Ablation study on NBHR test set for SpO₂

Training strategy	RMSE(%)↓	MAE(%)↓
Standard RMSE loss	2.74	1.96
Weighted RMSE (LDS)	2.30	1.77
Weighted RMSE plus time reversal augmentation	2.20	1.67

TABLE VII: Comparison of models for SpO₂ prediction on the PURE dataset

Model	Architecture	RMSE(%)↓
ST Maps plus EfficientNetB3	CNN based	26.80
RhythmMamba	ViM based	26.80
Modified PhysNet	3D CNNs	0.96

of-the-art models and falling within clinically allowable error ranges, thus highlighting its potential for real-time use in resource-constrained neonatal intensive-care units. By moving beyond traditional HR-only approaches and showing that neonatal SpO₂ can also be estimated using contact-free video, **VideoPulse** advances the field toward the practical deployment of camera-based neonatal vital-sign monitoring in clinical settings.

VIII. ACKNOWLEDGMENT

We thank Dr. Sheshan Mendis, Dr. M. H. M. Amjad, and the postnatal ward staff at De Soysa Maternity Hospital for their assistance with participant handling and clinical safety supervision during data acquisition.

REFERENCES

- [1] C.-H. Cheng, Z. Yuen, S. Chen, K.-L. Wong, J.-W. Chin, T.-T. Chan, and R. So, "Contactless blood oxygen saturation estimation from facial videos using deep learning," *Bioengineering*, vol. 11, no. 3, p. 251, 2024.
- [2] X. Liu, J. Fromm, S. Patel, and D. McDuff, "Multi-task temporal shift attention networks for on-device contactless vitals measurement," in *Adv. Neural Inf. Process. Syst. (NeurIPS)*, 2020.
- [3] L. Zhou, M. Guess, K. R. Kim, and W. H. Yeo, "Skin-interfacing wearable biosensors for smart health monitoring of infants and neonates," 12 2024.
- [4] International Organization for Standardization, "Medical electrical equipment — part 2-61: Particular requirements for basic safety and essential performance of pulse oximeter equipment," International Organization for Standardization, Tech. Rep. ISO 80601-2-61:2017, Dec. 2017, edition 2. Corrected version (en): 2018-02. [Online]. Available: <https://www.iso.org/standard/67963.html>
- [5] Association for the Advancement of Medical Instrumentation, "Cardiac monitors, heart rate meters, and alarms," Association for the Advancement of Medical Instrumentation, Tech. Rep. ANSI/AAMI EC13:2002, 2002, revision of ANSI/AAMI EC13:1992. [Online]. Available: <https://webstore.ansi.org/standards/aami/ansiaamiec132002>
- [6] W. Wang, A. C. den Brinker, S. Stuijk, and G. de Haan, "Algorithmic principles of remote ppg," *IEEE Trans. Biomed. Eng.*, vol. 64, no. 7, pp. 1479–1491, 2017.

- [7] X. Niu, H. Han, S. Shan, and X. Chen, "Synrhythm: Learning a deep heart rate estimator from general to specific," in *2018 24th International Conference on Pattern Recognition (ICPR)*, 2018, pp. 3580–3585.
- [8] C. Hu, K.-Y. Zhang, T. Yao, S. Ding, J. Li, F. Huang, and L. Ma, "An end-to-end efficient framework for remote physiological signal sensing," in *2021 IEEE/CVF Int. Conf. Comput. Vision Workshops (ICCVW)*, 2021, pp. 2378–2384.
- [9] J. Joshi and Y. Cho, "ibvp dataset: Rgb-thermal rppg dataset with high resolution signal quality labels," *Electronics*, vol. 13, no. 7, 2024. [Online]. Available: <https://www.mdpi.com/2079-9292/13/7/1334>
- [10] Z. Yu, X. Li, and G. Zhao, "Remote photoplethysmograph signal measurement from facial videos using spatio-temporal networks," in *Brit. Mach. Vision Conf. (BMVC)*, 2019.
- [11] W. Chen and D. McDuff, "Deepphys: Video-based physiological measurement using convolutional attention networks," in *Lecture Notes in Computer Science (including subseries Lecture Notes in Artificial Intelligence and Lecture Notes in Bioinformatics)*, vol. 11206 LNCS, 2018.
- [12] J. Speth, N. Vance, P. Flynn, and A. Czajka, "Non-contrastive unsupervised learning of physiological signals from video," in *2023 IEEE Conf. Comput. Vision Pattern Recognit. (CVPR)*, 2023, pp. 14464–14474.
- [13] Z. Yu, Y. Shen, J. Shi, H. Zhao, P. Torr, and G. Zhao, "Physformer: Facial video-based physiological measurement with temporal difference transformer," in *2022 IEEE Conf. Comput. Vision Pattern Recognit. (CVPR)*, 2022, pp. 4176–4186.
- [14] A. Gu and T. Dao, "Mamba: Linear-time sequence modeling with selective state spaces," 2024. [Online]. Available: <https://openreview.net/forum?id=AL1fq05o7H>
- [15] B. Zou, Z. Guo, X. Hu, and H. Ma, "Rhythmmamba: Fast remote physiological measurement with arbitrary length videos," *ArXiv*, vol. abs/2404.06483, 2024. [Online]. Available: <https://api.semanticscholar.org/CorpusID:269009998>
- [16] B. Huang, W. Chen, C.-L. Lin, C.-F. Juang, Y. Xing, Y. Wang, and J. Wang, "A neonatal dataset and benchmark for non-contact neonatal heart rate monitoring based on spatio-temporal neural networks," *Engineering Applications of Artificial Intelligence*, vol. 106, p. 104447, 2021.
- [17] A. Dasari, S. K. A. Prakash, L. A. Jeni, and C. S. Tucker, "Evaluation of biases in remote photoplethysmography methods," *npj Digital Medicine*, vol. 4, no. 1, p. 91, 2021. [Online]. Available: <https://doi.org/10.1038/s41746-021-00462-z>
- [18] W. Wang, A. C. den Brinker, S. Stuijk, and G. de Haan, "Algorithmic principles of remote PPG," *IEEE Transactions on Biomedical Engineering*, vol. 64, no. 7, pp. 1479–1491, 2017. [Online]. Available: <https://doi.org/10.1109/TBME.2016.2609282>
- [19] G. de Haan and V. Jeanne, "Robust pulse rate from chrominance-based rPPG," *IEEE Transactions on Biomedical Engineering*, vol. 60, no. 10, pp. 2878–2886, 2013. [Online]. Available: <https://doi.org/10.1109/TBME.2013.2266196>
- [20] V. A. A. van Es, R. G. P. Lopata, E. P. Scilingo, and M. Nardelli, "Contactless cardiovascular assessment by imaging photoplethysmography: A comparison with wearable monitoring," *Sensors*, vol. 23, no. 3, p. 1505, 2023. [Online]. Available: <https://doi.org/10.3390/s23031505>
- [21] F. Haugg, M. Elgendi, and C. Menon, "Effectiveness of remote PPG construction methods: A preliminary analysis," *Bioengineering*, vol. 9, no. 10, p. 485, 2022. [Online]. Available: <https://doi.org/10.3390/bioengineering9100485>
- [22] A. Dasari, S. K. Arul Prakash, L. A. Jeni, and C. S. Tucker, "Evaluation of biases in remote photoplethysmography methods," *npj Digital Medicine*, vol. 4, no. 1, p. 91, 2021. [Online]. Available: <https://doi.org/10.1038/s41746-021-00462-z>
- [23] B. Acharya, W. Saakyan, B. Hammer, and H. Drimalla, "The reliability of remote photoplethysmography under low illumination and elevated heart rates," *npj Digital Medicine*, vol. 8, no. 1, p. 744, 2025. [Online]. Available: <https://doi.org/10.1038/s41746-025-02192-y>
- [24] M. Lewandowska, J. Rumiński, T. Kocójko, and J. Nowak, "Measuring pulse rate with a webcam: A non-contact method for evaluating cardiac activity," in *Proceedings of the 2011 Federated Conference on Computer Science and Information Systems (FedCSIS)*, Szczecin, Poland, 2011, pp. 405–410. [Online]. Available: <https://annals-csis.org/proceedings/2011/pliks/188.pdf>
- [25] Y.-P. Yu, P. Raveendran, C.-L. Lim, and B.-H. Kwan, "Dynamic heart rate estimation using principal component analysis," *Biomedical Optics Express*, vol. 6, no. 11, pp. 4610–4618, 2015. [Online]. Available: <https://doi.org/10.1364/BOE.6.004610>
- [26] D. Wedekind, A. Trumpp, F. Gätjen, S. Rasche, K. Matschke, H. Malberg, and S. Zaunseeder, "Assessment of blind source separation techniques for video-based cardiac pulse extraction," *Journal of Biomedical Optics*, vol. 22, no. 3, p. 035002, 2017. [Online]. Available: <https://doi.org/10.1117/1.JBO.22.3.035002>
- [27] M.-Z. Poh, D. J. McDuff, and R. W. Picard, "Non-contact, automated cardiac pulse measurements using video imaging and blind source separation," *Optics Express*, vol. 18, no. 10, pp. 10762–10774, 2010. [Online]. Available: <https://doi.org/10.1364/OE.18.010762>
- [28] —, "Advancements in noncontact, multiparameter physiological measurements using a webcam," *IEEE Transactions on Biomedical Engineering*, vol. 58, no. 1, pp. 7–11, 2011. [Online]. Available: <https://doi.org/10.1109/TBME.2010.2086456>
- [29] G. R. Tsouri, S. Kyal, S. Dianat, and L. K. Mestha, "Constrained independent component analysis approach to nonobtrusive pulse rate measurements," *Journal of Biomedical Optics*, vol. 17, no. 7, p. 077011, 2012. [Online]. Available: <https://doi.org/10.1117/1.JBO.17.7.077011>
- [30] R. Macwan, Y. Benezeth, and A. Mansouri, "Remote photoplethysmography with constrained ICA using periodicity and chrominance constraints," *BioMedical Engineering OnLine*, vol. 17, no. 1, p. 22, 2018. [Online]. Available: <https://doi.org/10.1186/s12938-018-0450-3>
- [31] X. Niu, H. Han, S. Shan, and X. Chen, "Vipl-hr: A multi-modal database for pulse estimation from less-constrained face video," in *Lecture Notes in Computer Science (including subseries Lecture Notes in Artificial Intelligence and Lecture Notes in Bioinformatics)*, vol. 11365 LNCS, 2019.
- [32] X. Niu, X. Zhao, H. Han, A. Das, A. Dantcheva, S. Shan, and X. Chen, "Robust remote heart rate estimation from face utilizing spatial-temporal attention," in *Proceedings of the IEEE International Conference on Automatic Face & Gesture Recognition (FG)*, 2019.
- [33] Z. Yu, X. Li, P. Wang, and G. Zhao, "Transrppg: Remote photoplethysmography transformer for 3d mask face presentation attack detection," *IEEE Signal Process. Lett.*, vol. 28, pp. 1290–1294, 2021.
- [34] X. Liu, B. Hill, Z. Jiang, S. Patel, and D. McDuff, "Efficientphys: Enabling simple, fast and accurate camera-based cardiac measurement," in *Proceedings - 2023 IEEE Winter Conference on Applications of Computer Vision, WACV 2023*, 2023.
- [35] J. Peng, W. Su, H. Chen, J. Sun, and Z. Tian, "CL-SPO2Net: Contrastive learning spatiotemporal attention network for non-contact video-based SpO2 estimation," *Bioengineering*, vol. 11, no. 2, p. 113, Jan. 2024, published 24 Jan 2024; article number 113. [Online]. Available: <https://www.mdpi.com/2306-5354/11/2/113>
- [36] M. Villarroel, A. Guazzi, J. Jorge, S. Davis, P. Watkinson, G. Green, A. Shenvi, K. McCormick, and L. Tarassenko, "Continuous non contact vital sign monitoring in neonatal intensive care unit," *Healthcare Technology Letters*, vol. 1, no. 3, pp. 87–91, sep 2014. [Online]. Available: <https://doi.org/10.1049/htl.2014.0077>
- [37] M. Villarroel, S. Chaichulee, J. Jorge, S. Davis, G. Green, C. Arteta, A. Zisserman, K. McCormick, P. Watkinson, and L. Tarassenko, "Non-contact physiological monitoring of preterm infants in the Neonatal Intensive Care Unit," *npj Digital Medicine*, vol. 2, no. 1, p. 128, 2019. [Online]. Available: <https://doi.org/10.1038/s41746-019-0199-5>
- [38] Y. Ye, L. Pan, D. Yu, D. Gu, H. Lu, and W. Wang, "Notch rgb-camera based spo2 estimation: a clinical trial in neonatal intensive care unit," *Biomed. Opt. Express*, vol. 15, no. 1, pp. 428–445, Jan 2024. [Online]. Available: <https://opg.optica.org/boe/abstract.cfm?URI=boe-15-1-428>
- [39] I. Nishidate, R. Yasui, N. Nagao, H. Suzuki, Y. Takara, K. Ohashi, F. Ando, N. Noro, and Y. Kokubo, "Rgb camera-based simultaneous measurements of percutaneous arterial oxygen saturation, tissue oxygen saturation, pulse rate, and respiratory rate," *Frontiers in Physiology*, vol. Volume 13 - 2022, 2022. [Online]. Available: <https://www.frontiersin.org/journals/physiology/articles/10.3389/fphys.2022.933397>
- [40] Á. Nagy, P. Földesy, I. Jánoki, D. Terbe, M. Siket, M. Szabó, J. Varga, and Á. Zarándy, "Continuous camera-based premature-infant monitoring algorithms for nicu," *Applied Sciences*, vol. 11, no. 16, 2021. [Online]. Available: <https://www.mdpi.com/2076-3417/11/16/7215>
- [41] Y. Yang, K. Zha, Y.-C. Chen, H. Wang, and D. Katabi, "Delving into deep imbalanced regression," in *International Conference on Machine Learning (ICML)*, 2021.
- [42] R. Stricker, S. Muller, and H. M. Gross, "Non-contact video-based pulse rate measurement on a mobile service robot," in *IEEE RO-MAN 2014 - 23rd IEEE International Symposium on Robot and Human Interactive Communication: Human-Robot Co-Existence: Adaptive Interfaces and Systems for Daily Life, Therapy, Assistance and Socially Engaging Interactions*, 2014.
- [43] C. Hu, K. Y. Zhang, T. Yao, S. Ding, J. Li, F. Huang, and L. Ma, "An end-to-end efficient framework for remote physiological signal sensing,"

- in *Proceedings of the IEEE International Conference on Computer Vision*, vol. 2021-October, 2021.
- [44] Y. Souley Dosso, D. Kyrillos, K. J. Greenwood, J. Harrold, and J. R. Green, "NICUface: Robust neonatal face detection in complex NICU scenes," *IEEE Access*, vol. 10, pp. 62 893–62 909, 2022. [Online]. Available: <https://doi.org/10.1109/ACCESS.2022.3181167>
- [45] E. Grooby, C. Sitaula, S. Ahani, L. Holsti, A. Malhotra, G. A. Dumont, and F. Marzbanrad, "Neonatal face and facial landmark detection from video recordings," in *2023 45th Annual International Conference of the IEEE Engineering in Medicine & Biology Society (EMBC)*. IEEE, 2023, pp. 1–5. [Online]. Available: <https://doi.org/10.1109/EMBC40787.2023.10340960>
- [46] Y. Zhao, H. Zhu, Q. Shu, R. Huan, S. Chen, and Y. Pan, "Towards a deeper insight into face detection in neonatal wards," in *Medical Image Computing and Computer Assisted Intervention – MICCAI 2024*, ser. Lecture Notes in Computer Science, vol. 15005. Springer Nature Switzerland AG, 2024, pp. 702–712. [Online]. Available: https://doi.org/10.1007/978-3-031-72086-4_66
- [47] M. Feli, K. Kazemi, I. Azimi, Y. Wang, A. Rahmani, and P. Liljeberg, "End-to-end ppg processing pipeline for wearables: From quality assessment and motion artifacts removal to hr/hrv feature extraction," in *2023 IEEE International Conference on Bioinformatics and Biomedicine (BIBM)*. IEEE, 2023.
- [48] M. Feli, I. Azimi, A. Anzanpour, A. M. Rahmani, and P. Liljeberg, "An energy-efficient semi-supervised approach for on-device photoplethysmogram signal quality assessment," *Smart Health*, vol. 28, p. 100390, 2023.
- [49] Y. Wang, I. Azimi, K. Kazemi, A. M. Rahmani, and P. Liljeberg, "Ppg signal reconstruction using deep convolutional generative adversarial network," in *2022 44th Annual International Conference of the IEEE Engineering in Medicine & Biology Society (EMBC)*. IEEE, 2022, pp. 3387–3391.
- [50] K. Kazemi, J. Laitala, I. Azimi, P. Liljeberg, and A. M. Rahmani, "Robust ppg peak detection using dilated convolutional neural networks," *Sensors*, vol. 22, no. 16, p. 6054, 2022.
- [51] C. H. Cheng, Z. Yuen, S. Chen, K. L. Wong, J. W. Chin, T. T. Chan, and R. H. So, "Contactless blood oxygen saturation estimation from facial videos using deep learning," *Bioengineering*, vol. 11, 2024.
- [52] X. Niu, S. Shan, H. Han, and X. Chen, "Rhythmnet: End-to-end heart rate estimation from face via spatial-temporal representation," *IEEE Transactions on Image Processing*, vol. 29, pp. 2409–2423, 2020.
- [53] K. Li, X. Li, Y. Wang, Y. He, Y. Wang, L. Wang, and Y. Qiao, "Videomamba: State space model for efficient video understanding," 2024. [Online]. Available: <https://arxiv.org/abs/2403.06977>
- [54] R. Stricker, S. Muller, and H. M. Gross, "Non-contact video-based pulse rate measurement on a mobile service robot," *IEEE International Symposium on Robot and Human Interactive Communication*, pp. 1056–1062, 2014.